The Use of Combined Three-Dimensional Electron Back Scatter Diffraction and Energy Dispersive X-Ray Analysis to Assess the Characteristics of the Gamma/Gamma-Prime Microstructure in Alloy 720Li™

D.J. Child,
e-mail: d.child@lboro.ac.uk
G.D. West,
e-mail: g.west@lboro.ac.uk
R.C. Thomson (corresponding author)*
e-mail: r.c.thomson@lboro.ac.uk
Telephone: +44(0)1509 223155

Department of Materials, Loughborough University, Loughborough, Leicestershire, LE11 3TU, United Kingdom.

Abstract

Multiple three-dimensional reconstructions of a γ/γ' phase structure in Alloy 720Li have been carried out by employing a serial milling technique with simultaneous electron back scatter diffraction (EBSD) and energy dispersive x-ray (EDX) analysis data collection. Combining EBSD data with EDX is critical in obtaining maps to distinguish between the chemically differing, but crystallographically similar γ and γ' phases present in the alloy studied. EDX is shown to allow the differentiation of γ and γ' phases, with EBSD providing increased grain shape accuracy. The combination of data sources also allowed identification of coherent γ/γ' phase interfaces that would not be identified using solely EBSD or EDX. The study identifies a region of grain banding within the alloy, which provides the basis for a three-dimensional comparison and discussion of γ' phase size between coarse and fine grain regions, whilst also identifying coherent γ' phase interfaces, possible only using both EDX and EBSD systems simultaneously. The majority of the γ' phase lies in the range of 1-10 μm in non-banded regions, with a detectable particle size limit of 500 nm being established. The validity of the reconstruction has been demonstrated using an electron interaction volumes model, and an assessment of the validity of EBSD and EDX data sources is discussed showing γ' phase connectivity in all dimensions.

Keywords

Electron backscatter diffraction (EBSD), energy dispersive x-ray analysis (EDX), 3D reconstruction, gamma-gamma prime, phase connectivity, grain banding.

1. Introduction

Jet turbine engines used in modern civil aviation rely heavily on the development of high temperature nickel based alloys to gain improvements in performance and efficiency. Nickel based alloys are widely used for turbine disc applications due to their high temperature fatigue and creep resistance. In addition, they display good resistance to corrosion and oxidation under severe operating conditions. One such alloy used in turbine disc applications is alloy 720Li.

Alloy 720Li is a nickel-based alloy containing substantial amounts of chromium and cobalt. This imparts the strength necessary in discs to resist the high stresses from contact and rotational forces. The nominal composition of alloy 720Li is shown in Table 1. Alloy 720Li forms a non-cuboidal γ/γ' phase structure, typically containing 19 volume per cent primary γ' phase, with reported grain sizes in the range of 2-13 μm [1]. A finer distribution of tertiary γ' phase is also present, with particles of approximately 40 nm in size. However, this reference describes uniform microstructures produced by powder metallurgy processing routes. Alloy 720Li used in disc applications is commonly produced via mechanical methods, which can contribute to undesirable effects on grain size distributions. One such effect is 'banding', which describes microstructures containing the desired larger grain structure 'banded' by regions of much finer grain size [2, 3].

Ni	Cr	Co	Mo	Ti	Al	W
Bal.	16	14.8	3	5	2.5	1.25

Table 1. Nominal chemical composition of alloy 720Li in wt.% [4].

In some instances, the ability to deliberately form both large and fine grain structures, based on heat treatments, has proven advantageous, as shown by Mitchell et al. [5]. Coarse grains were developed to give good creep and fatigue crack growth resistance in the rim of a disc, whilst finer grains towards the bore impart optimised tensile and fatigue strengths. However, single microstructure components, such as those studied here, require a trade-off between the two behaviours. Recent studies [2] have shown the tendency of nickel based alloy to succumb to banding where a uniform grain size distribution is required. The occurrence of fine grain bands may reduce creep and fatigue crack growth resistance properties in these regions, due to alteration of the γ/γ' phase distribution [5, 6]. Identification and characterisation of such features are therefore advantageous in understanding the effects of banding on γ/γ' phase morphologies.

Quantitative analyses of γ/γ' phase distributions [7-9] have previously been limited to two dimensions, introducing a number of geometrical assumptions for three-dimensional estimation. Recent studies [10-13] have detailed serial milling techniques using focussed ion beam systems to tomographically reconstruct different phases. The reconstruction of γ/γ' phase structures in three dimensions has also been demonstrated [14-16], which allow observations of morphological aspects such as true particle shape and precipitate phase connectivity. However, such examples have only produced small scale reconstructions of cuboidal secondary γ' phase structures within volumes of 10 x 10 x 5 μm approximate dimensions. Other techniques, such as three-dimensional atom probe are also available [17], but are again suited to the study of small volumes.

This study aims to analyse a γ/γ' phase structure in alloy 720Li formed by wrought processing techniques over a larger volume of approximately 40 x 40 x 30 μm using a

serial milling technique. Data collection over a number of successive slices yields electron back scatter diffraction (EBSD), electron dispersive x-ray (EDX) and secondary electron (SE) data useable for three-dimensional phase reconstruction, using a computer-based tomography package. EDX maps are the primary data used to reconstruct γ' phase, because the chemistry differs between γ' phase and the γ matrix. Usually, EBSD data can be used in the same way by segmentation (the selection of desired phases) based on different crystal structures. However, in this instance, γ' and γ phases have almost identical crystal structures meaning differentiation between the two is impossible with current systems. γ phase is a Ni-based solid solution and displays a face-centred cubic structure, whilst γ' phase is an intermetallic phase displaying an $L1_2$ structure (in the form of Ni_3Al), with below 1% mismatch between the two, resulting in the difficulty in phase differentiation. Combination of EDX and EBSD data allows the discernment of phases from EDX with increased grain shape accuracy provided by EBSD, whilst also allowing distinction between coherent phases with EDX that would not be identified solely using EBSD. The study has also identified a region of grain banding within the alloy, which provides the basis for a three-dimensional comparison and discussion of γ' phase size between coarse and fine grain regions.

2. Experimental Procedure

2.1 Sample Preparation and Data Collection

The alloy 720Li sample used in this study was supplied as a 10 x 10 x 2 mm block from the centre of a wrought billet. This was mounted in conductive Bakelite and cut to reveal the cross-section of interest. Grinding and polishing operations to a 1 μm finish were then performed on the face of interest and its adjacent surface. The edge that these

two faces formed was carefully prepared to ensure it remained as sharp as possible at an angle of 80 degrees. This selection of angle has been found to allow for optimum serial sectioning over large distances.

The instrument used to perform the data collection was an FEI Nova 600 Nanolab Dual-Beam Field Emission Gun Scanning Electron Microscope (FEGSEM)/Focussed Ion Beam (FIB) system. Further sample preparation was necessary using the dual-beam instrument to avoid problems such as redeposition and shadowing during collection. Shadowing occurs when the electron signal recorded by the EBSD camera or the x-rays collected by the EDX detector are impeded from reaching their target, thus creating a 'shadow' in data maps of lost signal. Obstruction of the signal can be caused by sample geometry or can be due to redeposition of milled material gathering in undesirable locations around the region of interest. Redeposition can be controlled by milling of large trenches either side of the region of interest using the ion beam. Trench milling is followed by the deposition of a platinum layer on the adjacent face to aid slice cutting homogeneity. A secondary electron FEGSEM image, taken at a beam voltage of 10 kV, of the prepared sample in shown in Figure 1.

[File: Fig1.pdf]

Figure 1. Secondary electron FEGSEM image showing the prepared sample of alloy 720Li ready for serial milling and data acquisition.

The three-dimensional collection of EBSD, EDX and SE images relies on the accuracy of the piezo-electronic stage movement and accompanying beam shifts used by the microscope. The serial milling process involves alternate slicing away from the face of interest followed by EBSD and EDX data collection. This is achieved using a 180

degree stage rotation around a pre-specified 16 degree stage tilt. An image of the internal set-up of the microscope is shown in Figure 2.

The reason for the holder and stage tilts are apparent when considering Figure 3. The sample is placed on an angled holder so that the face of interest is pre-tilted to 54 degrees. Two different positions were used to perform slicing (Figure 3a) and data acquisition (Figure 3b). In the cutting position, the adjacent face is perpendicular to the ion beam column allowing a slice thickness of 250 nm to be removed. When the stage is rotated by 180 degrees, the face of interest is tilted at 70 degrees (54 degree holder tilt plus 16 degree stage tilt) in relation to the EBSD camera, which allows for optimum data collection. After collection, the stage is rotated back to the cutting position for another slice removal as the cycle repeats. An automated script allows the process to run unattended. Positional consistency is achieved by milling fiducial markers within the field of view on the adjacent face which are auto-aligned by the script using the microscope beam shifts. Each slice takes approximetely 50 minutes to complete. A total of 120 slices were collected, pertaining to a volume of 48000 μm^2 (40 x 40 x 30 μm) for the analysis presented in this paper.

[File: Fig2.pdf]

Figure 2. Chamberscope image showing the relative positions of the electron and focused ion beam columns and some of the various detectors within the FEI Nova 600 Nanolab Dual-Beam FEGSEM/FIB system.

[File: Fig3.pdf]

Figure 3. Schematic representations inside the dual-beam chamber showing (a) the cutting position used for slice removal, and (b) the data collection position used to collect EBSD, EDX and SE data from the face of interest.

EDX and EBSD data were collected simultaneously at a beam voltage of 20 kV, where the rate of acquisition was limited by EDX data collection to ensure chemical maps of high statistical accuracy. EDX data collection was achieved using an EDAX Silicon Drift Detector Apollo XL (SDD) at an input count rate of 325k counts per second and a processing time of 0.5 µs. These settings were optimised for the highest possible net peak intensity for chromium collection which was to be used to distinguish γ' and γ phases. Table 2 shows the expected elemental compositions of γ' and γ phase, collected from the respective regions in alloy 720Li using spot analysis with the EDX detector already specified. Elemental data shows γ' phase to be low in Cr and γ phase to be high in Cr. EBSD data were collected at a rate of 30 frames per second over an area measuring 40 x 40 µm with a step size of 0.2 µm, using an EDAX Hikari EBSD camera. The slice thickness was 250 nm. Both phases were indexed to a nickel structure file with a lattice parameter of 3.52 Å, to enable data processing using EDAX's TSL OIM software package. Due to the previously mentioned similarity between γ' and γ phase crystallography, the same structure file was used to identify both phases to avoid the software making a random phase choice, which would impede data processing. The run took approximately 90 hours to complete.

Phase	**Ni**	**Cr**	**Co**	**Mo**	**Ti**	**Al**
γ	56.1 ± 0.14	18.2 ± 0.18	16.2 ± 0.06	3.9 ± 0.02	3.5 ± 0.07	2.1 ± 0.04
γ'	70.7 ± 0.29	4.2 ± 0.29	9.2 ± 0.13	0.9 ± 0.11	10.5 ± 0.19	4.5 ± 0.06

Table 2. Average elemental compositions of γ' and γ phases in alloy 720Li in wt.%, as determined by EDX spot analysis on five different regions of each phase.

EBSD data are most commonly interpreted in terms of 'inverse pole figure' (IPF) maps. This assigns a particular colour for a specific orientation of a data point. The software used recognises separate grains based on user-specified constraints. In this paper, grains are defined by grain boundaries when the orientation change from one point to its neighbour is greater than five degrees in Eüler space. Confidence Index (CI) is also referred to in this paper, which is a measure of the degree of certainty the collection software has that a data point has been indexed correctly.

2.2 Data Validation

Electron interaction volumes can significantly affect the spatial resolution of EDX data from samples. In some cases, electrons producing x-ray signals for chemical data can penetrate several microns into sample surfaces, the extent of this penetration being termed the interaction volume. Large interaction volumes mean that the elemental presence of subsurface features (such as phases) is recorded, whilst also artificially broadening phases to greater areas than in reality. To assess the effects of the electron interaction volumes experienced during data collection, the computer simulation package 'CASINO' (monte CArlo SImulation of electroN trajectory in sOlids) [18] was used to replicate the experimental conditions as accurately as possible. CASINO was used to evaluate scanning across a γ'/γ phase interface. Conditions specified include the 70 degree sample tilt relative to the electron beam, the relative chemistries of the γ' and γ phases as determined by previous EDX (shown in Table 2) on the alloy and the correct beam voltage (20 kV).

2.3 Microstructural Reconstruction

For γ' phase reconstruction, the primary data source used was chromium EDX maps. In addition to the use of chromium EDX maps, maps from EBSD data were also generated. Once extracted from the data, the consecutive slices of chromium elemental distribution maps were aligned, by a least contrast method.

The method used to distinguish between γ' and γ phases in EDX maps was histogram thresholding between two predefined pixel grey values. Segmentation was performed using Avizo version 6.0.0 [19]. In some cases, notably, with EBSD data maps, segmentation was performed by a manual selection of individual grains for each slice, rather than the automated volume selection possible by thresholding grey values in EDX data. This was because EBSD data maps (such as inverse pole figures), often provide unambiguous grain boundary location information, but these alone do not allow determination of γ' phase from γ phase, due to their very similar crystallography. The detection threshold for grain boundaries was chosen to represent an orientation difference greater than five degrees between adjacent data points.

3. Results

3.1 Data collection

The dataset collected was free from artefacts, with no effect of shadowing from redeposition and a high confidence index (64 per cent of data had a confidence index above 0.6, with the most common confidence index being 0.93) of EBSD data. A selection of data maps extracted from a single slice is shown in Figure 4, which includes an inverse pole figure (IPF) map showing a two-dimensional representation of absolute orientation, an image quality (IQ) map (a measure of EBSD pattern intensity) , a grain

boundary map, and EDX-derived distribution maps of chromium, titanium and molybdenum. The EDX-derived distribution map of chromium is particularly useful in this instance because it highlights γ' phase as being lower in chromium content than γ phase, owing to the $Ni_3(Al, Ti)$ chemistry of γ' phase. Such EDX information is critical in this dataset because it is very difficult to identify the γ' phase from any of the EBSD-based maps available (Figures 4(a-c)). Chromium maps (total counts ~ 290) are used in preference to titanium (total counts ~ 205) and molybdenum (total counts ~ 100) maps because of the superior x-ray count ratio between gamma and gamma-prime phases. All of the maps in Figure 4 are useful in showing differences between fine and coarse grain regions resulting from banding, indicated in the figure.

COLOUR[File: Fig4.pdf]

Figure 4. Extracted data maps from the combined EBSD/EDX serial milling technique showing maps for: (a) inverse pole figure, (b) image quality, (c) grain boundaries, EDX-derived distribution maps of (d) chromium, (e) titanium, (f) molybdenum (light = high counts, dark = low counts), in slice 80 out of 120.

3.2 Examination of Reconstruction Accuracy

In order to make conclusions regarding the phase connectivity of the γ' phase in the alloy studied, it is necessary to firstly validate the accuracy of the collected data used for reconstructions. To investigate this aspect, CASINO was used to simulate the scanning of a γ'/γ phase interface at 70 degrees sample tilt relative to the electron beam. A graphical representation of the electron interaction volume close to a γ'/γ phase interface is shown in Figure 5. The percentages in the key of Figure 5 refer to the percentage of electrons that penetrate to a greater extent than the region defined by the line. γ' and γ

phase elemental compositions were determined by EDX on the respective regions of alloy 720Li. The elemental compositions are shown in Table 2. Two chromium x-ray intensity profiles simulating an electron beam scanning across a γ/γ' phase interface and also a γ'/γ interface are shown in Figure 6. Chromium x-ray intensity profiles simulating a scan across different-sized γ' phases, in order to assess the theoretical limitations of the spatial resolution of the EDX data collected, are shown in Figure 7, which also includes a thresholding line at 176 counts which represents the contrast threshold used in Avizo to identify γ' phase.

[File: Fig5.pdf]

Figure 5. CASINO simulation of the electron interaction volume of a 20 kV electron beam, close to a γ'/γ phase interface, based on the percentage of electrons within the defined regions (see key).

[File: Fig6.pdf]

Figure 6. CASINO simulation of Cr EDX counts collected from a 20 kV electron beam scanning across an (a) γ/γ' phase interface and (b) γ'/γ phase interface, where position 0 is the defined boundary between γ' and γ phases.

[File: Fig7.pdf]

Figure 7. CASINO simulation of Cr EDX counts collected from a 20 kV electron beam scanning across γ' phases of sizes 10, 100, 1000, 2000 nm centred about the zero position, showing the 'reconstruction contrast threshold' used to reconstruct γ' phases in Avizo.

Figure 8 builds on Figure 7 by using it to compare the specified particle size to the theoretical particle size when reconstructed from chromium EDX data. For example, using the reconstruction contrast threshold in Figure 7 applied to a 1 μm diameter γ'

phase, it is predicted that this is reconstructed as a 765 nm diameter particle, thus displaying a 24 per cent diameter loss, as displayed in Figure 8. Above 1-2 μm particle diameter, a loss of below 20 per cent is observed and above 6 μm in particle diameter it is found that error of approximately five per cent occurs.

[File: Fig8.pdf]

Figure 8. Percentage diameter loss of differently-sized γ' phase based on the reconstruction contrast threshold shown in Figure 7, using CASINO simulations of Cr EDX counts collected from a 20 kV electron beam scanning.

3.3 Three-Dimensional Reconstruction

The initial reconstruction of the γ' phase used chromium EDX maps (as shown in Figures 5 and 6(d) for single slices). The γ' phase reconstruction obtained from all 120 data slices is shown in Figure 9, bounded by a wire frame of 40 x 30 x 40 μm dimensions. The reconstruction is orientated so that slice 1 is at the front of the perspective.

[File: Fig9.pdf]

Figure 9. Three-dimensional reconstruction of γ' phase segmented from 120 consecutive chromium energy dispersive x-ray maps, from a section of alloy 720Li, using a serial milling technique (slice thickness 250 nm).

Two specific volumes within this larger reconstruction (each representing approximately 10 per cent of the total volume of the reconstruction), are displayed in Figure 10, showing the difference between coarse and fine regions. The bounding boxes in Figure 10 represent the same volume (25 x 20 x 10 μm) for both coarse and fine grain regions.

[File: Fig10.pdf]

Figure 10. Three-dimensional reconstruction of γ' phase segmented from chromium energy dispersive x-ray maps, from a section of alloy 720Li, showing a: (a) coarse grain region; (b) fine grain region.

3.4 Phase Connectivity and Exploration of Data Processing Routes

A useful post-processing step enables EDX and EBSD data to be truly combined using EDAX's TSL OIM processing software [20]. A series of three maps of the same slice, demonstrating the production of an average EDX count per grain map, is shown in Figure 11(c), which is therefore a combination of EBSD (grain shape) and EDX (phase identification) data. Based on the grains identified using the EBSD data (where a grain is identified by a threshold by a boundary angle difference of five degrees and more than two data points), an average number of chromium EDX counts over each grain is assigned. A higher number of average counts results in a higher greyscale value for the whole grain. In regions displaying coherent interfaces, the reconstruction reverts to using EDX data to distinguish between phases. A series of these maps can be used in building a three-dimensional reconstruction as before, and are shown in Figure 12.

[File: Fig11.pdf]

Figure 11. Data maps from a combined EDX/EBSD serial milling technique data collection from an alloy 720Li section, from slice 87 out of 120, showing: (a) image quality data; (b) chromium EDX data; (c) combined average EDX count per grain data.

A comparison between the datasets from four different map sources showing a γ' phase reconstructed portion, is shown in Figure 12. The standard chromium EDX map and

the titanium EDX maps are included in Figure 12(a) and (b) respectively. EBSD grain boundary maps and average EDX count data per grain maps are shown in Figure 12(c) and Figure 12(d) respectively. Titanium maps were used in addition to chromium maps because the gamma prime phase is rich in titanium but low in chromium. A combination of EBSD and EDX data for segmentation is demonstrated in Figure 12(d), by the grain average EDX count data maps. A comparison of the volumes in Figure 12 shows that there is no significant visual difference between reconstructions from different datasets. Volumes of reconstructed γ' phase are quantified for each data source in Table 3.

[File: Fig12.pdf]

Figure 12. Various three-dimensional reconstructions of the same γ' phase volume, within a section of alloy 720Li, from different data map sources: (a) chromium EDX, (b) Titanium EDX, (c) EBSD grain boundary, (d) average EDX count data per grain. The feature labelled i indicates an interconnected region.

Reconstruction Data Source	**Reconstructed volume / voxels**
Cr EDX	1997635
Ti EDX	2033484
Grain boundary EBSD	2103934
Average EDX count per grain	2466289

Table 3. Volume statistics of reconstructed γ' phase using a serial milling technique, from a alloy 720Li section, from four different data sources. Reconstructed volumes are displayed in Figure 12 of this paper.

The IPF maps, shown in Figures 6(a) and 7(a) can be used to show that the complex shapes of γ' phase precipitates are a collection of interconnected grains rather than a single grain of complex geometry. IPFs are used in preference to unique grain colour maps (for example) because the maps are comparable from one slice to the next. The orientation of a grain should remain fairly consistent throughout the slices in which it is present; whereas a unique grain colour would have no comparability as grain colour would change randomly for each slice. Figure 13 shows a series of IPF maps from the reconstructed volume in Figure 12. For clarity, the grains of interest, identified as γ' phase from the EDX maps, are shown in colour against the desaturated (black and white conversions of the original coloured grains) γ phase.

COLOUR[File: Fig13.pdf]

Figure 13. A series of inverse pole figure maps from a combined EDX/EBSD serial milling technique data collection from a alloy 720Li section, showing: (a) slice 83; (b) slice 85; (c) slice 86; (d) slice 87, out of 120 slices. Grains of interest are identified as γ' phase from EDX maps, and are labelled in (d) from 1 to 6, remaining in colour in contrast to the desaturated γ phase.

3.5 Phase Coherency

One final aspect to consider is the appearance of coherent phase interfaces between γ and γ' phases. All reconstructions on selected areas made so far have been in regions where γ' phase has consisted of the whole grain. Other areas, especially in the fine grain regions, show a strong presence of coherent interfaces separating γ' and γ phases that are not identified by EBSD, but are shown by EDX maps due to the elemental differences between the phases. An example of γ' phase bounded coherently within a γ phase grain is shown in Figure 14.

COLOUR[File: Fig14.pdf]

Figure 14. Data maps showing an identical scan area within a section of alloy 720Li, demonstrating the presence of coherent γ' phase, with maps: (a) colour chromium EDX; (b) inverse pole figure + image quality with grain boundary identification; (c) colour chromium EDX + image quality with grain boundary identification, where 'ii' identifies a coherent phase.

4. Discussion

4.1 Reconstruction Validity

The use of CASINO has aided greatly in providing validity for the accuracy of the γ' phase reconstruction. The cross-sectional distribution of electrons within the alloy volume is shown in Figure 5. The figure shows that less than 10 per cent of electrons scatter to an extent greater than approximately 250 nm, and only 5 per cent of electrons scatter into the surface deeper than 590 nm. Therefore, it can be concluded that x-ray generation contributing to the EDX signal is confined to thicknesses comparable to the slices analysed (250 nm). With the grey scale threshold used to reconstruct γ' phase, a γ' phase particle would be identified in a γ phase surface only if it was as close as 60 nm to the analysed surface.

CASINO simulation scans across γ'/γ and γ/γ' phase interfaces are provided by Figures 7(a) and (b). The simulation shows the intensity of x-ray signal being generated as would be observed in a map used for three-dimensional reconstruction. As the scan approaches the γ' phase at the zero position there is a drop in signal beginning some 800 nm prior to the defined boundary, as the interaction volume dictates in Figure 6(a). Figure 6(b) shows the reverse situation whereby the signal rises again approximately

800 nm before the actual defined edge of the γ' phase. The error depends on the thresholding point of the chromium EDX profiles. The threshold value used for the reconstructions is represented in Figure 7 as 176 counts on the x-ray intensity, relating to a grey value of 105 (on a scale from 0 to 255) used in Avizo. As particle size increases, the percentage loss of actual particle diameter compared to the reconstructed particle diameter decreases, as shown in Figure 8. The percentage error is highest below a 1 μm particle diameter, but rapidly decreases and levels out at low values above 1 μm diameter. It is therefore still possible to gain valid quantitative results from the data collected, if γ' phase sizes are corrected using the calibration curve shown in Figure 8. The particle size detection limit for this technique appears to be 500 nm, indicated by the asymptotic nature of the relationship shown by the line of best fit through points in Figure 8.

4.2 Grain Banding Effects

The two-dimensional maps allow an understanding of the grain structure present in alloy 720Li, including both γ and γ' phases. Grain banding is evident in the later slices of the dataset (for example in the lower left corner of slice 80 in Figure 5).

The full-scale representation of γ' phase in Figure 9 demonstrates an impressive ability to reconstruct larger volumes in three-dimensions, but segmentation of coarse and fine grain volumes is also possible, and is shown in Figure 10. It is clearly observable that there is a difference in γ' phase grain size.

4.3 Evaluation of Reconstruction Data

The data used for reconstruction are shown in Figure 11, with their subsequent reconstructions evaluated in Figures 14 and 15. The first comparison to consider is the EDX data source. EDX maps from both chromium and titanium were used for the reconstructions displayed in Figure 12(a) and (b). Titanium was chosen in addition to chromium because it is more abundant in the γ' phase (due to the Ni_3(Al, Ti) structure of γ' phase), and can be compared with chromium, which is abundant in the γ phase. Chromium is abundant in γ phase, where the low count regions are segmented, and titanium is abundant in γ' phase, where the high count region is therefore segmented. Due to any interaction volume effect that may be present, it would be expected that regions of high counts would appear enlarged against their actual size, due to the spread of electron interaction. For chromium maps this would mean that γ phase is enlarged which could impinge on the γ' phase volume. For titanium, γ' phase may be enlarged due to this effect. However, if Figures 15(a) and (b), and Table 2, are compared, it is observed that the reconstructed volumes are both visually and statistically very similar. This would suggest that a significant interaction volume effect is not present in this case.

Construction of the third model shown in Figure 12(c), was the most time consuming of the four. A manual selection of each grain had to be made by identifying γ' phase grains using chromium EDX maps. Using EBSD however, allowed a more accurate representation of the limits of each grain as this data source more clearly shows grain boundaries. Much more time efficient was the combined EDX/EBSD data showing the average EDX counts per grain, shown in Figure 12(d). The combined dataset allowed for easy identification and selection of γ' phase grains, as with the EDX data, but grain shape detail was maintained, unlike with the EDX data. The combined EDX/EBSD

dataset therefore provided the most accurate three dimensional reconstruction of γ' phase in the alloy, and fully realised the integration of the two types of recorded data.

4.4 Phase Connectivity

The apparent connectivity of γ' phase through an analysed volume is demonstrated in Figures 14 and 15. The comparison with EBSD data is critical in determining whether phases are in fact connected in three dimensions or whether this is an effect of electron beam interaction volume. Observing Figure 12(a) shows a region labelled 'i' where connectivity is observed where it perhaps appears to be an artefact of signal spread due to interaction volume effects. Comparing this feature in Figures 15(a) and (b) from EDX to (c) purely from EBSD shows that in fact the γ' phase grains identified from EDX are indeed adjoined in reality in the XY plane. Connectivity is further confirmed by the combined EDX/EBSD data in Figure 12(d). The resolution in the XY plane is determined by the spatial resolution of the EDX detector settings in use (a 200 nm step size). In the YZ plane, shown in Figure 12, the limiting resolution factor is the slice thickness used (250 nm in this study). The slice thickness used results in a voxel size of 1 x 1 x 1.25, therefore there is slightly increased resolution in XY compared to the slice direction YZ. Phase connectivity in the YZ plane is therefore resolvable to 250 nm, which is adequately detailed to confirm connectivity in this slicing plane. An assessment of the shape shows the cross section of such areas to be fairly consistent through the slicing direction, only ceasing at the particle ends. It could therefore be concluded that such features are in fact one elongated grain through the volume. This argument is countered by observing the progression of individual grains through the slicing direction in Figure 13. Using the grain identities labelled in Figure 13(d),

connectivity in both the XY and the YZ and XZ planes can be observed. Firstly, connectivity in the XY plane can be again proven by the contact between grains 3, 4 and 5 through Figures 16(b) to (d). In Figure 13(b) the grains are distinctly separate, a fact confirmed by EDX. In Figure 13(c) grains 4 and 5 connect, and in Figure 13(d) all three grains are connected. In the Z plane, grain 1 provides a suitable example. In Figure 13(a) grain 1 is separated from any other γ' phase grain. However, through Figures 16(b) to (d) the connectivity with grain 2 is increasingly observed, which consequently joins with grain 3. Therefore, it can be concluded that the γ' phase grains are indeed interconnected in three dimensions.

4.5 Coherent Interfaces

The identification of coherent interfaces provides further justification for a combined EDX/EBSD data run, as absence of either of these datasets results in coherent interfaces being unidentified. A coherent γ/ γ' phase interface is illustrated in Figure 14(a), in which a number of γ' phases can be identified by their lack of chromium (in blue to blue green). Incoherent grain interfaces in black (and twin boundaries in yellow) are shown from the EBSD data in Figure 14(b). Combining the two data types in Figure 14(c) shows a feature labelled ‘ii’ as γ' phase within a larger grain consisting mainly of γ phase. EBSD records no boundary (defined as a change in orientation greater than five degrees in Eüler space) between the two regions and so it is deemed coherent. A number of examples of coherent interfaces between γ and γ' phases are present throughout the dataset, more noticeably in the fine grain regions. It was previously stated that the most representative three-dimensional reconstruction of γ' phase was achievable using a combined dataset, allowing segmentation from average EDX count

data per grain. In regions displaying coherent interfaces, the reconstruction is achieved with EDX data, rather than combined data, to distinguish between phases. Such flexibility with the data highlights the advantages of combined EDX/EBSD collection.

5. Summary

The capability to perform a large-scale microstructural reconstruction has been demonstrated in a nickel based superalloy material consisting of γ' and γ phases. This surpasses other examples of γ' phase segmentation in terms of scale and is believed to provide the first three-dimensional reconstruction of primary γ' phase, including both EBSD and EDX data.

The validity of the three-dimensional reconstruction has been demonstrated using CASINO to model electron interaction volumes. Simulations show that no significant chromium EDX signal can be obtained from any distance greater than the slice thickness (250 nm) or indeed greater than 60 nm. The majority of γ' phase particles have sizes which lie in the range of 1-10 μm in non-banded regions, which experience a diameter loss through reconstruction of approximately 5 per cent, which is easily accounted for in quantitative calculations. A detectable particle limit of 500 nm has been established.

The techniques used allowed the observation of grain banding in three-dimensions to reveal the fine grain distribution present in these regions. Reconstruction of the banded region enables the quantification of particle volume, diameter and shape in both fine and coarse regions from comparison.

Reconstruction has been shown to be most representative of reality with a combination of EDX and EBSD data. Using both sources of data allows identification of γ' phase grains using EDX data whilst maintaining the shape accuracy of the grain from EBSD data. The increased detail and flexibility of the data justifies the use of the combined methodology so that EDX can be used for distinguishing between phases that have similar crystallography, such as γ' and γ phases, in nickel based alloys. Furthermore, it was found that any interaction volume effect possible with EDX data did not significantly affect results by artificially reducing or increasing the volume modelled as γ' phase.

Phase connectivity of the γ' phase was confirmed in all dimensions of the reconstructed volume, most easily proven in the XY plane, and using IPF data maps to demonstrate this in the Z plane. Connectivity of the phases was shown not to be affected by the data source used for reconstruction.

Coherent interfaces were identified in the volume studied using a combination of the EDX and EBSD datasets, which would otherwise have been overlooked had only one of the two datasets been available, i.e. distinction of phases is not possible without EDX data, but identification of coherent phase interfaces is not possible without EBSD data. This does introduce constraints if reconstructing using combined EDX and EBSD data, but provides an addition justification for using the two systems in tandem.

In summary, using this large-scale serial milling technique, the alloy studied provides an excellent grain size distribution for analysis, with the region studied being ideally suited for evaluation of banding effects in three dimensions. An assessment of the validity of different data sources has been discussed which confirms γ' phase

connectivity in all dimensions, whilst also identifying coherent γ' phase interfaces, possible only using both EDX and EBSD systems simultaneously.

Acknowledgements

We would like to thank J. Leggett, G. Gibson and D. R. Rickerby from Rolls-Royce plc., Derby, for their valuable input into this work.

References

[1] H.T. Pang, P.A.S. Reed, Fatigue crack initiation and short crack growth in nickel-base turbine disc alloys - the effects of microstructure and operating parameters, International Journal of Fatigue. 25 (2003) 1089-1099.

[2] C. Dumont, J. Thebault, D. Solas, B. Tie, C. Rey, T. Baudin, Ultrasonic Inspectability and Modelling of Microstructure Evolution During Hot Working in a Nickel-base Superalloy, Aubert & Duval. (2010).

[3] H. Monajati, M. Jahazi, R. Bahrami, S. Yue, The influence of heat treatment conditions on γ′ characteristics in Udimet™ 720, Materials Science and Engineering A. 373 (2004) 286-293.

[4] S.E. Kim, M.P. Jackson, R.C. Reed, C. Small, A. James, N.K. Park, Quantification of the minor precipitates in UDIMET™ alloy720(LI) using electrolytic extraction and X-ray diffraction, Materials Science and Engineering A. 245 (1998) 225-232.

[5] R.J. Mitchell, J.A. Lemsky, R. Ramanathan, H.Y. Li, K.M. Perkins, L.D. Connor, Process Development & Microstructural & Mechanical Property Evaluation of a Dual Microstructure Heat Treated Advanced Nickel Disc Alloy, (2008) 347-356.

[6] D.A. Woodford, Gas phase embrittlement and time dependent cracking of nickel based superalloys, Energy Materials. 1 (2006) 59-79.

[7] A. Szczotok, J. Richter, J. Cwajna, Stereological characterization of γ′ phase precipitation in CMSX-6 monocrystalline nickel-base superalloy, Mater Charact. 60 (2009) 1114-1119.

[8] J. Wosik, B. Dubiel, A. Kruk, H. Penkalla, F. Schubert, A. Czyrska-Filemonowicz, Stereological estimation of microstructural parameters of nickel-based superalloy Waspaloy using TEM methods, Mater Charact. 46 (2001) 119-123.

[9] J.S. Tiley, G.B. Viswanathan, A. Shiveley, M. Tschopp, R. Srinivasan, R. Banerjee, H.L. Fraser, Measurement of γ′ precipitates in a nickel-based superalloy using energy-filtered transmission electron microscopy coupled with automated segmenting techniques, Micron. 41 (2010) 641-647.

[10] J. Konrad, S. Zaefferer, D. Raabe, Investigation of orientation gradients around a hard Laves particle in a warm-rolled Fe_3Al-based alloy using a 3D EBSD-FIB technique, Acta Materialia. 54 (2006) 1369-1380.

[11] M. Schaffer, J. Wagner, B. Schaffer, M. Schmied, H. Mulders, Automated three-dimensional X-ray analysis using a dual-beam FIB, Ultramicroscopy. 107 (2007) 587-597.

[12] R. Wirth, Focused Ion Beam (FIB) combined with SEM and TEM: Advanced analytical tools for studies of chemical composition, microstructure and crystal structure in geomaterials on a nanometre scale, Chem. Geol. 261 (2009) 217-229.

[13] G.D. West, R.C. Thomson, Combined EBSD/EDX tomography in a dual-beam FIB/FEG-SEM, Journal of Microscopy. 233 (2009) 442-450.

[14] A.C. Lund, P.W. Voorhees, The effects of elastic stress on microstructural development: the three-dimensional microstructure of a γ–γ′ alloy, Acta Materialia. 50 (2002) 2585-2598.

[15] J. MacSleyne, M.D. Uchic, J.P. Simmons, M. De Graef, Three-dimensional analysis of secondary γ′ precipitates in René-88 DT and UMF-20 superalloys, Acta Materialia. 57 (2009) 6251-6267.

[16] M.D. Uchic, M. De Graef, R. Wheeler, D.M. Dimiduk, Microstructural tomography of a Ni70Cr20Al10 superalloy using focused ion beam microscopy, Ultramicroscopy. 109 (2009) 1229-1235.

[17] R.C. Thomson, M.K. Miller, Atom probe characterisation of high temperature materials, Materials Science and Technology. 16 (2000) 1199-1206.

[18] D. Drouin, A.R. Couture, R. Gauvin, P. Hovington, P. Horny, H. Demers, CASINO (monte CArlo SImulation of electroN trajectory in sOlids), 2.42 (2001).

[19] Mercury Computer Systems SAS, Avizo (Build: “snapshot”), 6.0.0 (2009).

[20] EDAX, TSL Crystallography Orientation Imaging Microscopy (OIM), 5.31 (2008).

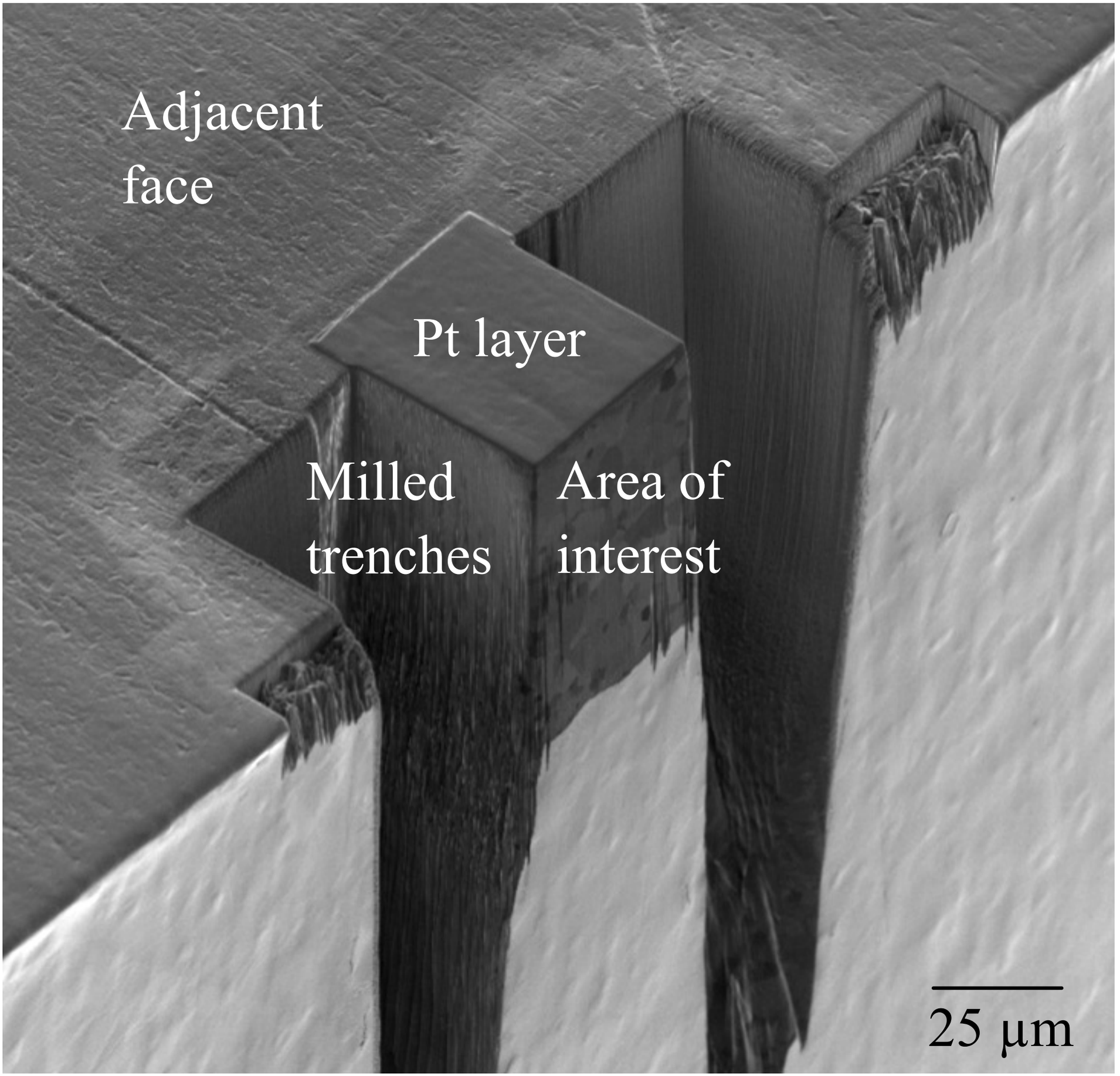
Adjacent face
Pt layer
Milled trenches
Area of interest
25 µm

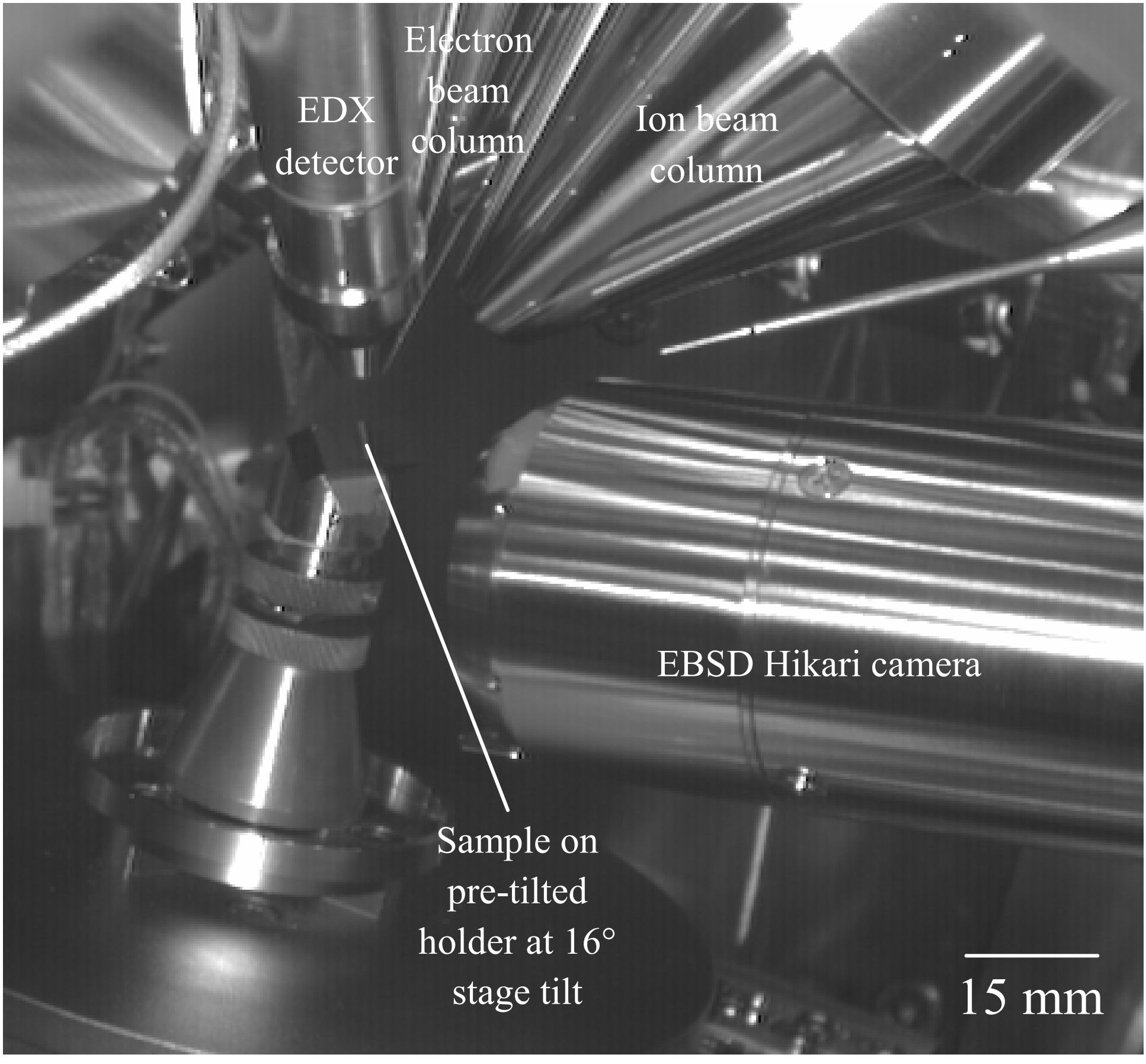
Electron
beam
column
EDX
detector
Ion beam
column
EBSD Hikari camera
Sample on
pre-tilted
holder at 16°
stage tilt
15 mm

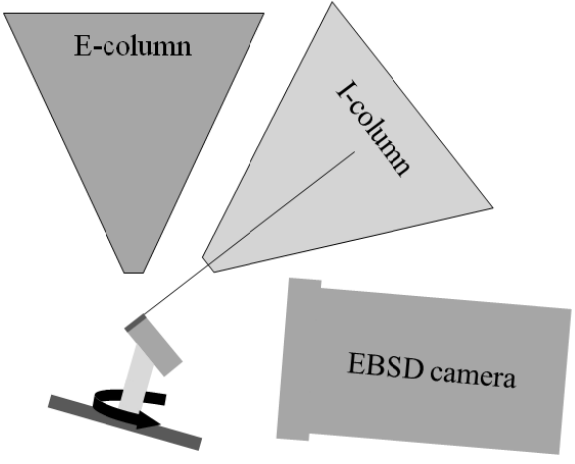

(a) Cutting position (Ion beam)

16° (stage tilt) + 36° (pre-tilt) = 52°

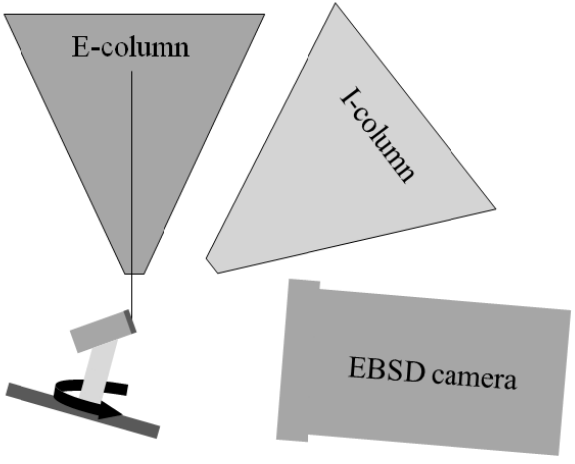

(b) EBSD/EDX position (Electron beam)

16° (stage tilt) + 54° (pre-tilt) = 70°

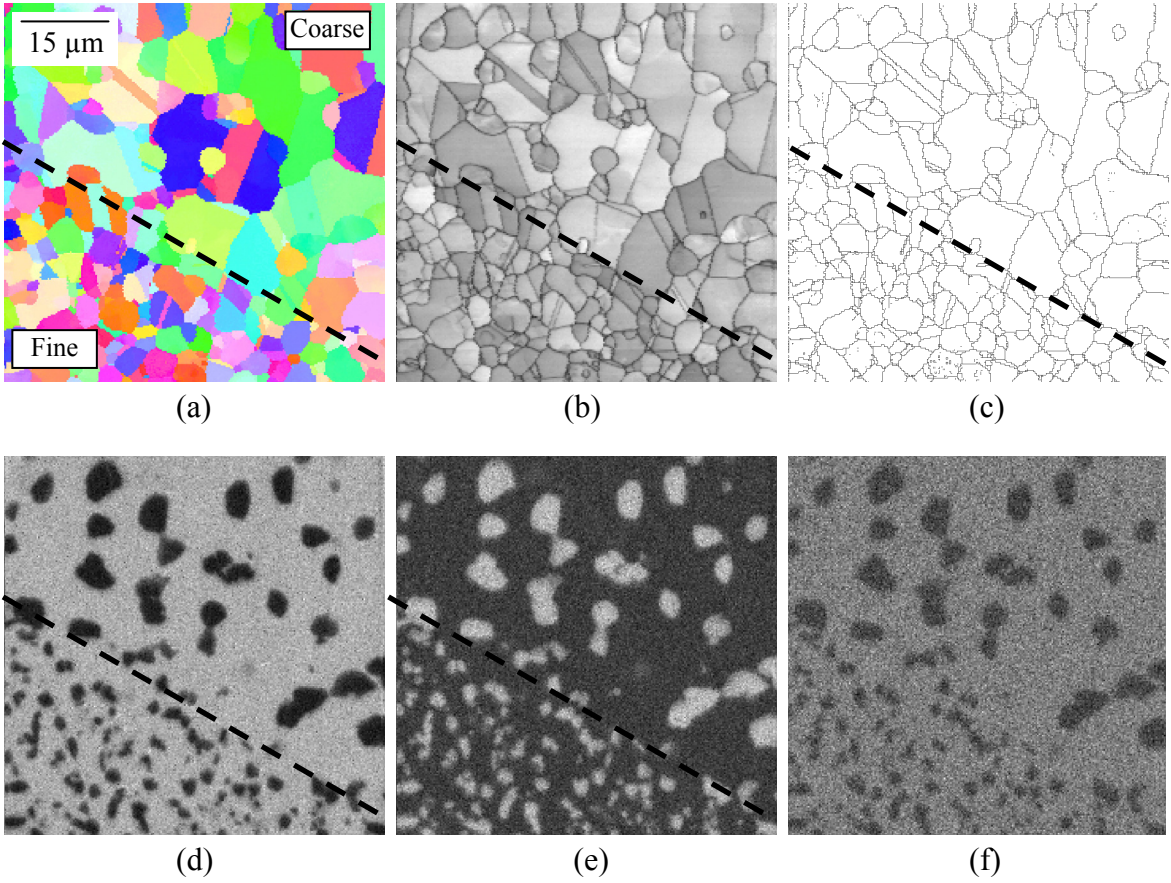
15 µm
Coarse
Fine
(a)
(b)
(c)
(d)
(e)
(f)

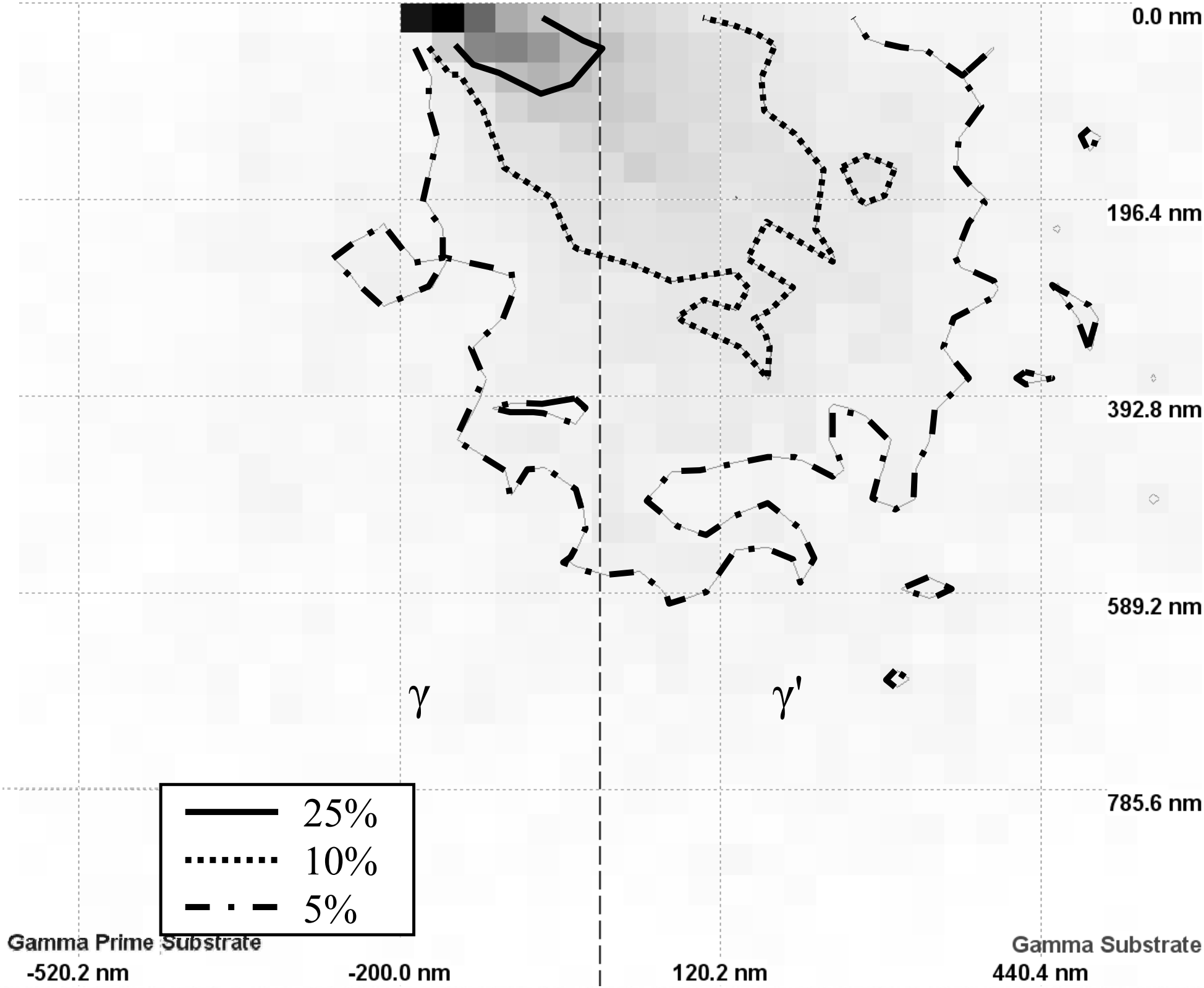
0.0 nm
196.4 nm
392.8 nm
589.2 nm
785.6 nm
γ
γ'
25%
10%
5%
Gamma Prime Substrate
Gamma Substrate
-520.2 nm
-200.0 nm
120.2 nm
440.4 nm

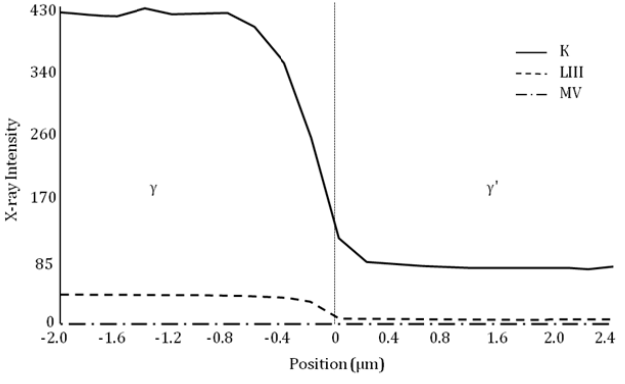
430
340
260
170
85
0
X-ray Intensity
K
LIII
MV
γ
γ'
-2.0
-1.6
-1.2
-0.8
-0.4
0
0.4
0.8
1.6
2.0
2.4
Position (μm)

(a)

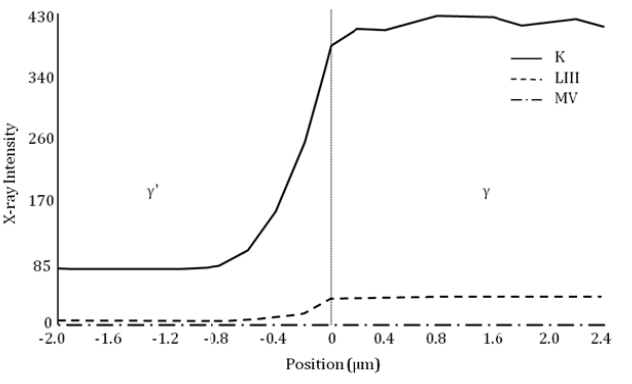
430
340
260
170
85
0
X-ray Intensity
K
LIII
MV
γ'
γ
-2.0
-1.6
-1.2
-0.8
-0.4
0
0.4
0.8
1.6
2.0
2.4
Position (μm)

(b)

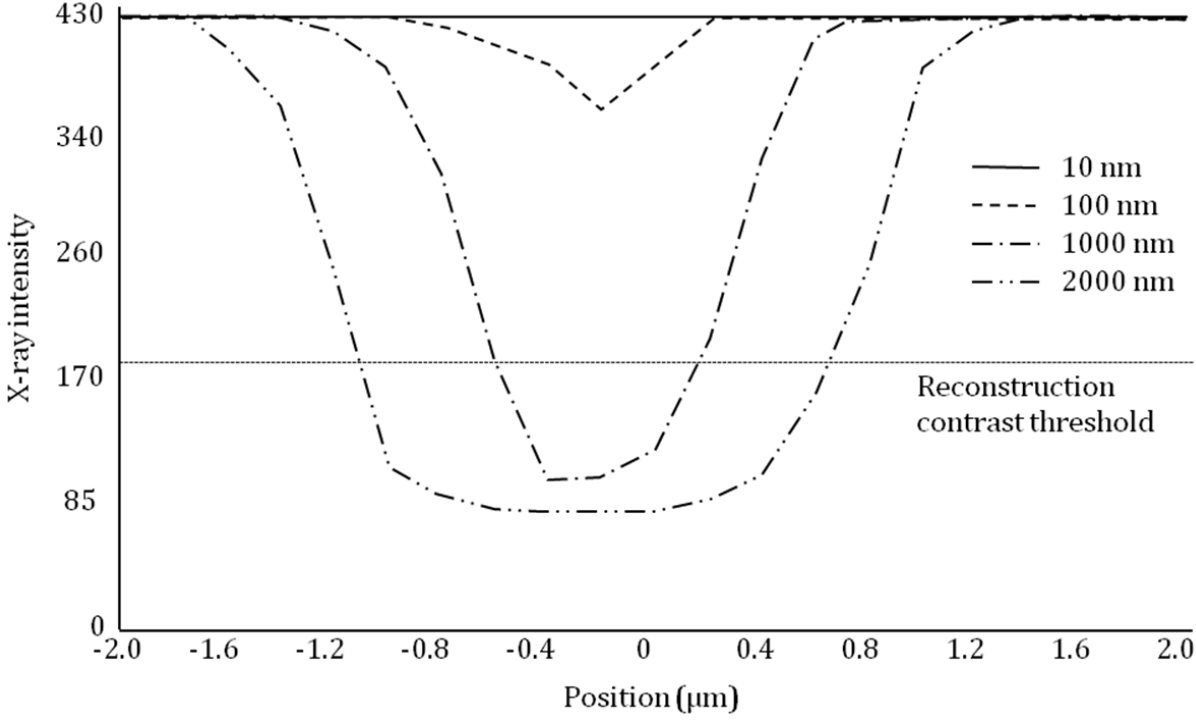
430
340
260
170
85
0
X-ray intensity
-2.0
-1.6
-1.2
-0.8
-0.4
0
0.4
0.8
1.2
1.6
2.0
Position (μm)
10 nm
100 nm
1000 nm
2000 nm
Reconstruction
contrast threshold

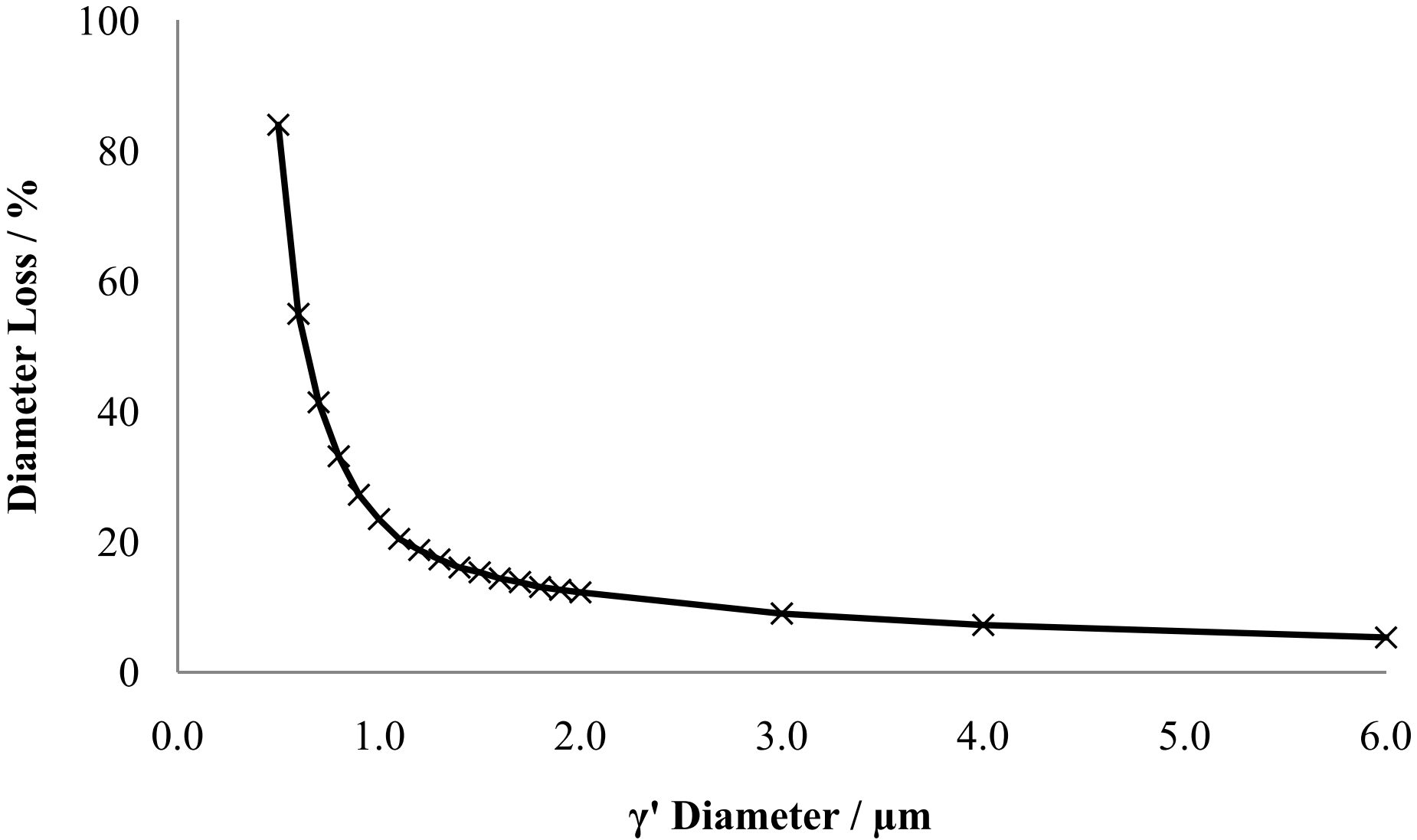
100
80
60
40
20
0
Diameter Loss / %
0.0
1.0
2.0
3.0
4.0
5.0
6.0
γ' Diameter / µm

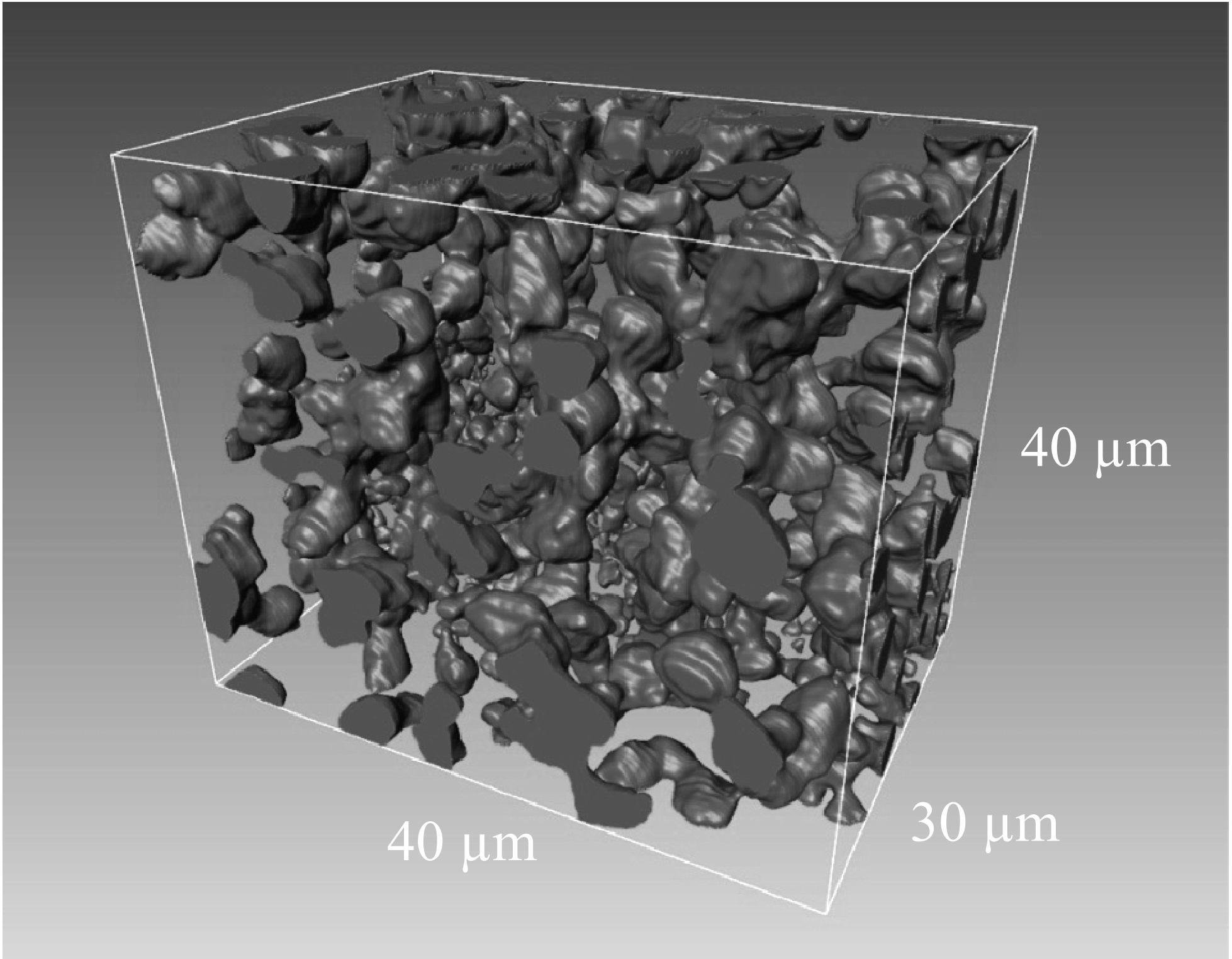
40 μm
40 μm
30 μm

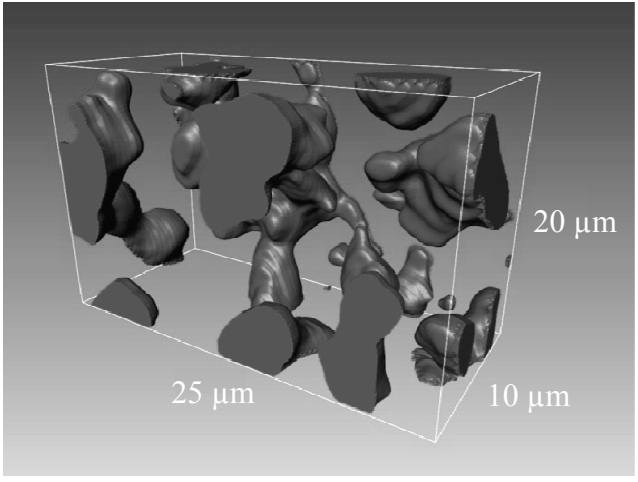

(a)

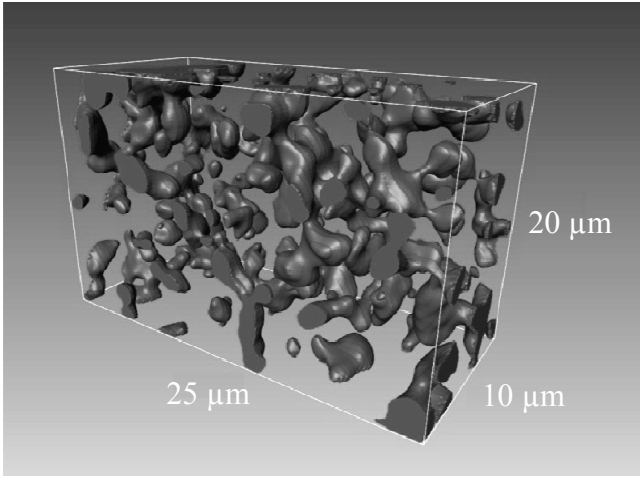

(b)

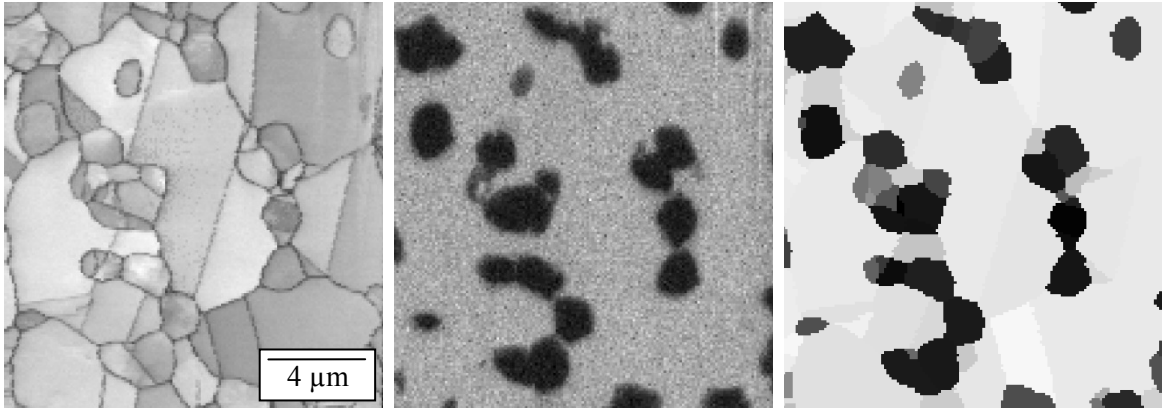

(a) (b) (c)

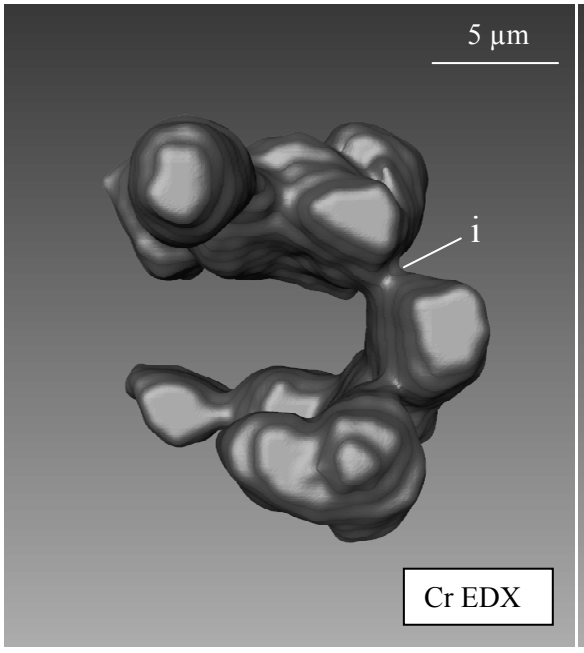

(a)

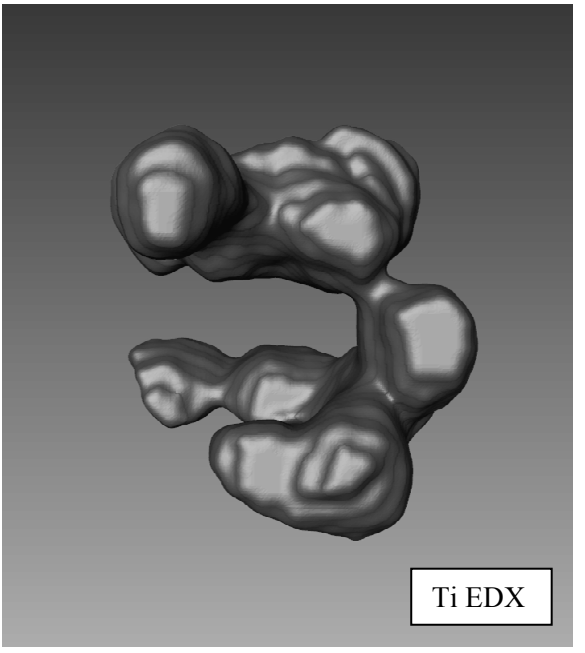

(b)

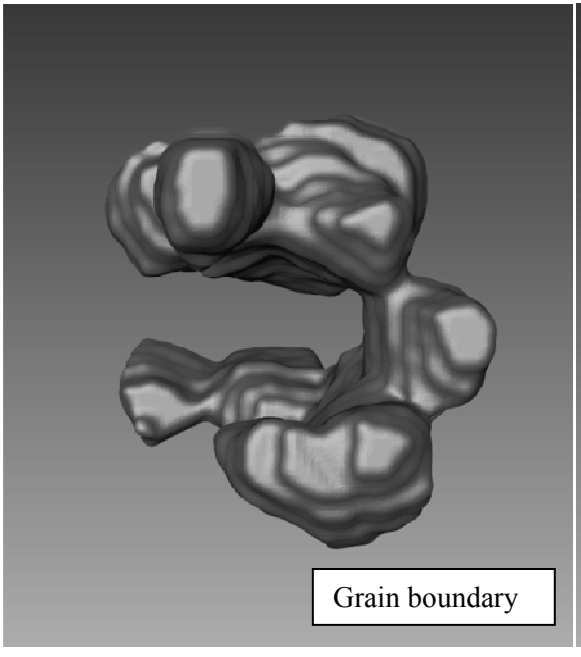

(c)

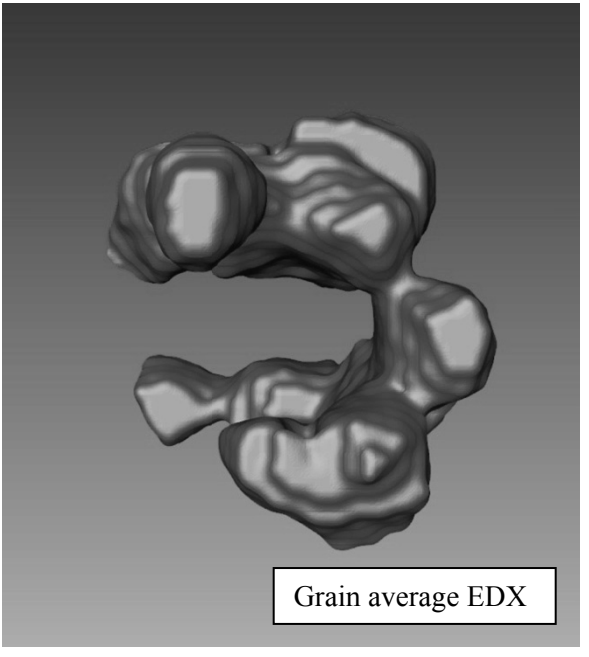

(d)

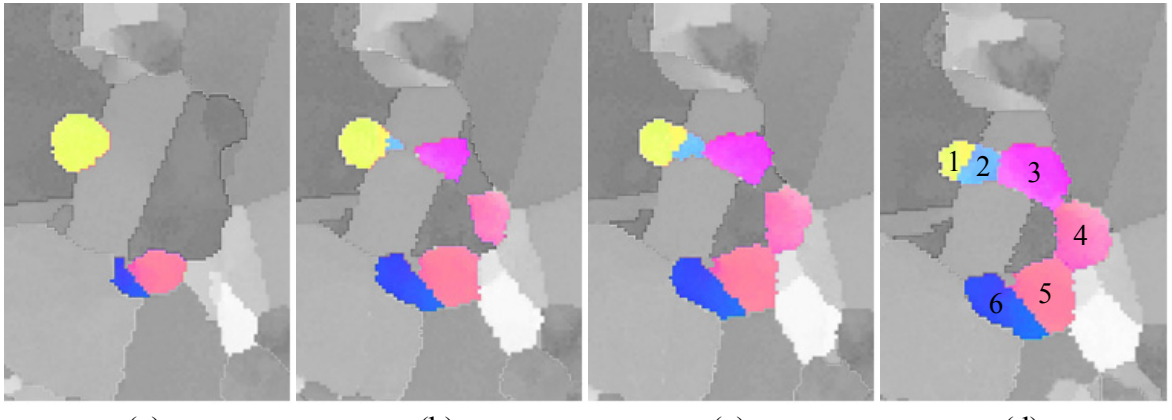

(a) (b) (c) (d)

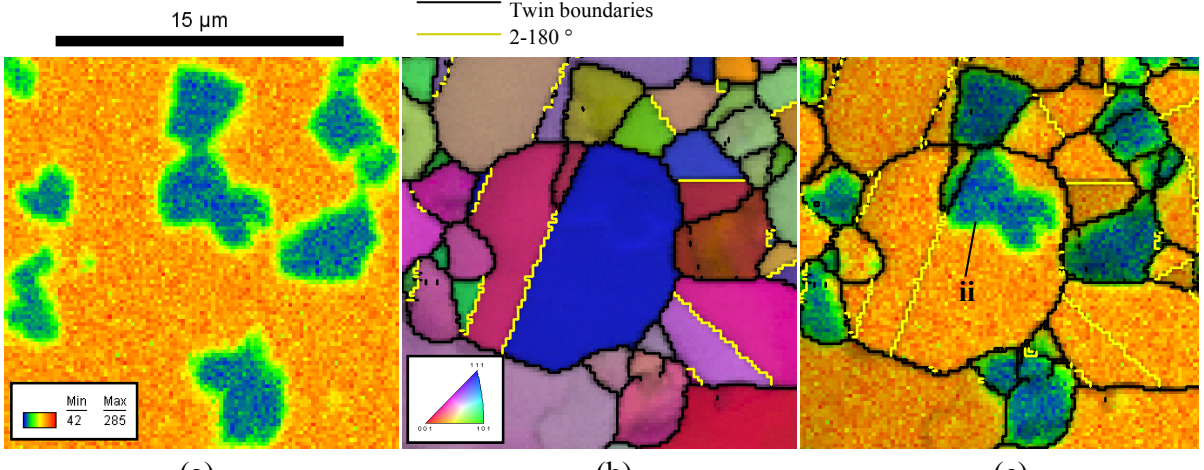
15 µm
Twin boundaries
2-180 °
Min
Max
42
285
111
001
101
ii
(a)
(b)
(c)